Available online at www.sciencedirect.com

ScienceDirect

journal homepage: www.elsevier.com/locate/he

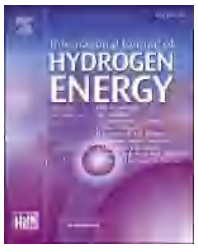

New mechanism and improved kinetics of hydrogen absorption and desorption of Mg(In) solid solution alloy milling with CeF_3

H.C. Zhong [a,b,*], *H.J. Lin* [c], *X.J. Lu* [a,b], *C.Y. Cao* [a,b], *C. Chen* [b], *J.J. Sun* [b]

[a] *Fujian Provincial Key Laboratory of Functional Materials and Applications, Xiamen University of Technology, Xiamen, 361024, China*

[b] *School of Materials Science and Engineering, Xiamen University of Technology, Xiamen, 361024, China*

[c] *Institute of Advanced Wear & Corrosion Resistance and Functional Materials, Jinan University, Guangzhou, 510632, China*

HIGHLIGHTS

- Nanostructured $CeIn_3$ forms by hydrogenation.
- In-situ formed $CeIn_3$ impedes the agglomeration of MgIn.
- Mg(In, Ce) solid solution reversibly forms by de/hydrogenation.
- The reversible phase transition and $CeIn_3$ enhance de/hydriding reaction.
- Destabilization/lowering dehydriding enthalpy of MgH_2 is achieved.

ARTICLE INFO

Article history:
Received 22 May 2019
Received in revised form
27 June 2019
Accepted 13 July 2019
Available online 14 August 2019

Keywords:
Hydrogen absorption and desorption
Mg-based solid solution
Phase transition
CeF_3
Nanocomposite
Mechanical milling

ABSTRACT

This paper presents improving the hydrogen absorption and desorption of Mg(In) solid solution alloy through doped with CeF_3. A nanocomposite of $Mg_{0.95}In_{0.05}$-5 wt% CeF_3 was prepared by mechanical ball milling. The microstructures were systematically investigated by X-ray diffraction, scanning electron microscopy, scanning transmission electron microscopy. And the hydrogen storage properties were evaluated by isothermal hydrogen absorption and desorption, and pressure-composition-isothermal measurements in a temperature range of 230 °C–320 °C. The mechanism of hydrogen absorption and desorption of $Mg_{0.95}In_{0.05}$ solid solution is changed by the addition of CeF_3. $Mg_{0.95}In_{0.05}$-5 wt % CeF_3 nanocomposite transforms to MgH_2, MgF_2 and intermetallic compounds of MgIn and $CeIn_3$ by hydrogenation. Upon dehydrogenation, MgH_2 reacts with the intermetallic compounds of MgIn and $CeIn_3$ forming a pseudo-ternary Mg(In, Ce) solid solution, which is a fully reversible reaction with a reversible hydrogen capacity ~ 4.0 wt%. The symbiotic nanostructured $CeIn_3$ impedes the agglomeration of MgIn compound, thus improving the dispersibility of element In, and finally improving the reversibility of hydrogen absorption and desorption of Mg(In) solution alloy. For $Mg_{0.95}In_{0.05}$-5 wt% CeF_3 nanocomposite, the dehydriding enthalpy is reduced to about 66.1 ± 3.2 kJ·mol^{-1}·H_2, and the apparent activation energy of dehydrogenation is significantly lowered to 71.9 ± 10.0 kJ·mol^{-1}·H_2, a reduction of ~ 73 kJ·mol^{-1}·H_2 relative to that for $Mg_{0.95}In_{0.05}$ solid solution. As a result, $Mg_{0.95}In_{0.05}$-5 wt% CeF_3 nanocomposite can release ~ 57% H_2 in 10 min at 260 °C. The

* *Corresponding author*. School of Materials Science and Engineering, Xiamen University of Technology, Xiamen, 361024, PR China.
E-mail address: hczhong@xmut.edu.cn (H.C. Zhong).

https://doi.org/10.1016/j.ijhydene.2019.07.114

improvements of hydrogen absorption and desorption properties are mainly attributed to the reversible phase transition of Mg(In, Ce) solid solution combing with the multiphase nanostructure.

Introduction

Hydrogen as a clean and renewable energy carrier is an ideal substitution to current fossil fuels for satisfying the requirements of sustainable society [1,2]. One of key issues for the commercial applications of hydrogen energy, e.g., hydrogen fuel cell vehicles, is the efficient and safe hydrogen storage technologies [3]. The light-weight hydrides are generally regarded as the ultimate solution to the delivery and storage of hydrogen [2,3]. Over last decades, various hydrides, such as MgH_2, $LiBH_4$, NH_3BH_3 etc, have been developed as potential hydrogen storage materials [4–8]. Unfortunately, those high-capacity hydrides always suffer from over high thermodynamic stability and/or sluggish kinetics that result in impractical high operating temperature for on-board applications [9–11].

Magnesium as one of the most promising hydrogen storage materials, has many outstanding advantages, such as high capacity, good cycle stability, abundant resource, low cost, and environmentally friendly. But the high thermodynamic stability of MgH_2 (−74.6 kJ·mol^{-1}·H_2) results in the high desorption temperature about 280 °C under a pressure of 1 bar H_2, and which will be further increased by the unfavorable kinetics due to the high activation energy barriers [12,13]. Recently, tremendous efforts have been made to lower the desorption temperature and improve the kinetics, such as alloying [13–16], doping catalysts [17–20], nanocrystallization and compositing [21–23], and achieving great progresses. For example, Yu et al. [24] synthesized MgH_2 nanocrystals together with catalytic Ni nanoparticles on the graphene, this MgH_2 nanocrystals presented fast hydrogen desorption rate at 200 °C, and could be re-hydrogenated at room temperature. Using a similar synthetic route, Li et al. [25] prepared Mg_2NiH_4 single crystal nanoparticles covered by a thin layer (~3 nm) of MgO, this nanostructured Mg_2NiH_4 exhibited a low desorption activation energy of 31.2 kJ·mol^{-1}·H_2, and high structural stability during hydrogen absorption and desorption. It was considered that MgO played a critical role in keeping the thermal stability of Mg_2Ni single crystal, and improving the hydrogen absorption and desorption properties [25]. The dimension effects were also confirmed in MgH_2@CA microspheres composite which released hydrogen with an activation energy of 114.8 kJ·mol^{-1}·H_2 [26]. It is generally regarded that nanocrystallization shortens the diffusion distance, decreases the thickness of H_2-impermeable layer of MgH_2, even weaken the Mg–H bonds, thus improving the kinetics. Doping catalytic additives, such as transition metals (Fe, Co, Ni, Cu, Ti, Nb, etc) [19,27,28], various nanosized metal oxides (TiO_2, V_2O_5, Cr_2O_3, Fe_2O_3, Nb_2O_5, etc) [18,20,29], fluorides/halides (TiF_3, $TiCl_3$, LaF_3, $LaCl_3$, CeF_3, $CeCl_3$, etc) [30,31], and so on, is widely used to enhance the de/hydriding kinetics. The comparative study indicated that elemental V had the best catalytic effect on dehydrogenation of MgH_2 among Ti, Mn, Fe and Ni [32]. For 0.75Mg-0.25Ti–H composite, the dehydriding activation energy was reduced to 53.6 kJ·mol^{-1}·H_2 [33]. Recently some multi-component oxides-$TiVO_{3.5}$, $SrTiO_3$ and $BaFe_{12}O_{19}$, were investigated as catalysts for de/hydrogenation of Mg [34–36]. Interestingly MgO was also found to have positive effect on enhancing the hydrogen absorption and desorption in some additives doped Mg systems, e.g. $MgNiO_2$ and $MgFe_2O_4$ doped MgH_2 systems [37,38]. Furthermore, the synergistic catalytic effects were found in some nanocomposite additives, e.g. the desorption temperature of MgH_2 was reduced to 210 °C due to the introduction of symbiotic $CeH_{2.73}$/CeO_2 nanocomposite [39]. Other approaches to improve the kinetics include forming composites with other hydrogen storage materials or reactive additives, e.g. AlH_3, $ZrFe_2H_x$, $ZrMn_2$ [23,40,41]. For example, MgH_2 + 10 wt% nano-$ZrMn_2$ composite showed a low desorption temperature of 181.9 °C, and reduced dehydrogenation activation energy ~83 kJ·mol^{-1}·H_2 [41]. Although crucial progresses have been achieved in improving the kinetics, the thermodynamic destabilization of MgH_2 is still facing big challenge at present.

With respect to thermodynamic destabilization, several strategies, namely nanostructuring, compositing with reactive additives, and alloying, have been employed [6,9,12,13,15,42,43]. Theoretically the stability of MgH_2 can be obviously lowered when the crystal size is reduced to less than 1.3 nm [44]. Nevertheless it is difficult to prepare this nanostructured Mg/MgH_2. Furthermore, owing to the high surface energy, the original nanoparticles always tend to grow and aggregate, which is particularly obvious during the consecutive thermal treatments for H_2 absorption and desorption, based on the solid-state reactions involving mass transport, leading to a quick loss of the nanostructured morphology and continuing deterioration of storage properties. Another innovative method is altering the de/hydriding reaction pathways. Representative example is MgH_2–Si system, which shows a significantly reduced dehydriding enthalpy of 36.4 kJ·mol^{-1}·H_2 due to the changed reaction route owing to the formation of Mg_2Si [42]. However, the reverse reaction was severely restricted by the high stability of Mg_2Si [42]. Additionally, forming intermetallic compounds by alloying with metal elements (e.g. Mg_2Ni, Mg_3MnNi_2) are effective approaches to tune the thermodynamics. Unfortunately these approaches are always suffered from a severe penalty of large capacity losses [45].

Mg-based solid solutions, performed minor modulations to the structure and composition of Mg, could be an alternative choice to avoid excessive capacity loss. Numerous works

demonstrated the improvements of hydrogen storage properties for Mg-base solid solutions, such as Mg–Ti/Co/Ni BCC/FCC structure solid solutions, metastable Mg–Y and Mg–Y–Ni supersaturated solid solutions by rapid solidification, and the equilibrium Mg–Li and Mg–Sc solid solutions [46–49]. However, those Mg-based solid solutions, whether in equilibrium or non-equilibrium state, could not recover from the hydrogenated products consisting of elemental hydrides and/or intermetallic compounds [50]. For instances, the supersaturated Mg–Y–Ni and Mg–Y–Zn solid solutions were irreversibly decomposed to MgH_2, YH_2/YH_3, Mg_2NiH_4 and/or $Mg_2Zn/MgZn_2$ by hydrogenation [48,49], and the equilibrium Mg–Li solid solution was irrecoverably hydrogenated to MgH_2 and LiH [50]. To the best of our knowledges, most of Mg-based solid solutions for hydrogen storage were limited by the unavoidable phase separation and poor structural reversibility.

Recently, it was confirmed that Mg(In) solid solutions could reversibly absorb and desorb hydrogen with lowered dehydriding enthalpy [6,51]. However, the intermetallic compound of MgIn (precipitated by hydrogenation) was easy to agglomerate, thus resulting in composition inhomogeneous, and further lowering the reaction rate of reforming Mg(In) solid solution, which deteriorated the de/hydriding kinetics [51]. As far as we know, Rare-earth fluorides/halides were confirmed to have catalytic effects on hydrogen absorption and desorption of Mg based alloys. Ismai et al. investigated the catalytic effects of $CeCl_3$ and $LaCl_3$ on MgH_2, and considered the in situ formed Ce/La–Mg alloys and $MgCl_2$ as active species to catalyze hydrogen absorption and desorption of Mg [52,53]. On the other hand, it was regarded that the addition of Rare-earth fluorides could modify the microstructures and reduce the agglomeration/growth of nano Mg particles, thus improving the hydrogen storage properties [31]. Herein, cerium fluoride (CeF_3) was doped to Mg(In) solid solution synthesized a nanocomposite of $Mg_{0.95}In_{0.05}$-5 wt% CeF_3 by ball milling. It was found that the nanostructured intermetallic compound of $CeIn_3$ instead of cerium hydrides ($CeH_2 \sim CeH_3$) formed by hydrogenation of $Mg_{0.95}In_{0.05}$-5 wt% CeF_3 nanocomposite, and this nanostructured $CeIn_3$ could limit the agglomeration of MgIn. Upon dehydrogenation, pseudo-ternary Mg(In, Ce) solid solution formed with reduced dehydriding enthalpy of 66.1 ± 3.2 kJ mol^{-1} H_2, and crucially lowered apparent activation energy of 71.9 ± 10.0 kJ mol^{-1} H_2 comparing with that for Mg(In) solid solution [51]. The results provide a new approach to improve the hydrogen storage properties of Mg based alloys.

Experimental details

Mg(In) binary solid solution was prepared by sintering and subsequent ball milling process. Firstly, powder mixtures of elemental Mg and In (99.9% purity, 200 meshes, Grinm Advanced Materials Co., Ltd., China) with designed composition of $Mg_{0.95}In_{0.05}$ (atomic ratio) were homogenized by ball milling, then pressed into pellets and sintered for 5 h at 573 K in a tube furnace under the protection of high purity argon (99.9999%) atmosphere. Secondly, the pellets were pulverized and milled with 5 wt% CeF_3 (99.9% purity, 300 meshes, Alfa Aesar) on a planetary mill (QM-3SP2, China) under the protection of high purity argon atmosphere. The weight ratio of powders to stainless steel balls was 1:50. To prevent temperature over rising, the milling program was interrupted for 30 min after continuously running for 30 min. Finally, a nanocomposite of $Mg_{0.95}In_{0.05}$-5 wt% CeF_3 was gotten by ball milling for 20 h.

The powders X-ray diffraction (XRD) was performed on the PANalytical X'Pert MRD diffractometer with Cu-Kα radiation ($\lambda = 1.54056$ Å). The morphology and phase distribution were observed by scanning electron microscope (SEM, ZEISS Sigma 500 attached OXFORD X-Max^N EDS) and scanning transmission electron microscopy (STEM, FEI TALOS F200S attached BRUKER Super-X EDS). The hydrogen storage properties were characterized by the measurements of pressure-composition isotherm (PCI) and isothermal hydrogen absorption and desorption on an automatic Sievert-type apparatus (homemade). The powders sample with a weight of 0.4000 g was sealed in a sample holder and loaded into a stainless steel vessel for the following hydrogen absorption and desorption measurements. Firstly, the apparatus pipelines system and sample chamber were evacuated for about 30 min. Then the program began to calibrate the volume of sample chamber at room temperature and target temperature using high purity argon. And then the measurements started according to the pre-set programs. Before the data collection, the sample was activated completely by undergoing 5 cycles of hydrogen absorption and desorption at 300 °C. The isothermal hydrogen absorption was carried out under an initial hydrogen pressure of 2.5 MPa. The hydrogen desorption kinetic measurements started in near vacuum condition.

Results and discussions

Morphology and de/hydriding transition

Fig. 1 presents the phase components of $Mg_{0.95}In_{0.05}$-5 wt% CeF_3 nanocomposite in different states. Fig. 1(a) is the XRD

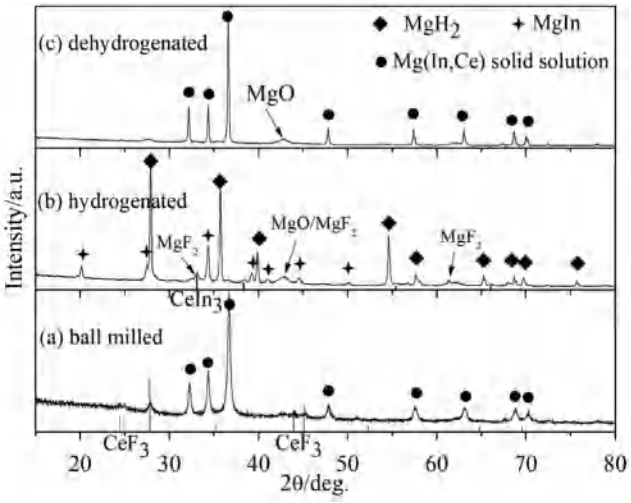

Fig. 1 – XRD patterns of ball milled $Mg_{0.95}In_{0.05}$-5 wt% CeF_3 nanocomposite. (a) ball milled, (b) hydrogenated, (c) dehydrogenated.

pattern of ball milled powders, which shows two phases of primitive Mg(In) solid solution and the doped CeF_3. By hydrogen absorption, the diffraction peaks of Mg(In) solid solution and CeF_3 were all disappeared accompanying with the appearances of the diffraction peaks of MgH_2 and intermetallic compounds of MgIn and $CeIn_3$, and traces of MgO and MgF_2 could be also observed, as illustrated in Fig. 1(b). Fig. 1(c) is the XRD pattern of dehydrogenated $Mg_{0.95}In_{0.05}$-5 wt% CeF_3 nanocomposite, in which only Mg together with trace of MgO could be observed. The intermetallic compounds of MgIn and $CeIn_3$ could have been decomposed by dehydrogenation, however there were no other new phases concerning In and Ce observed. So it is believed that MgIn and $CeIn_3$ have reacted with MgH_2 forming a pseudo-ternary Mg(In, Ce) solid solution by dehydrogenation, which is similar with the reversible de/hydriding mechanism of Mg(In) binary solid solution. However, there was an interesting phenomenon that the cerium fluoride (CeF_3) did not react with H_2 forming cerium hydrides (e.g. CeH_2 and CeH_3) as reported in other materials systems [30,31].

For understanding the microstructures of $Mg_{0.95}In_{0.05}$-5 wt % CeF_3 nanocomposite, SEM and STEM were performed to observe the morphology and microstructures, the results are illustrated in Figs. 2–4. Fig. 2 is the back scattering electron images of $Mg_{0.95}In_{0.05}$-5 wt% CeF_3 nanocomposite. From Fig. 2(a) and Fig. 2(b), it can be observed that the particle size of ball milled powders is in several micrometer degree. However, CeF_3 (the bright particles marked by arrows in Fig. 2(a)) was

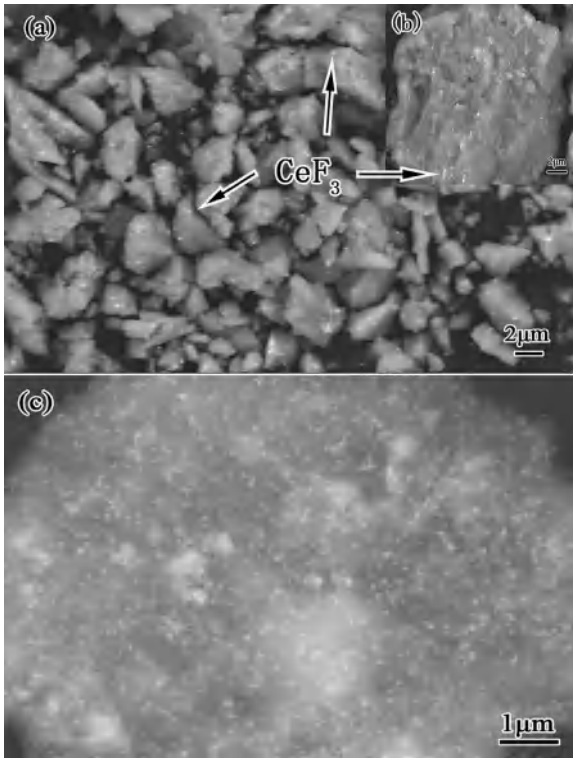

Fig. 2 – SEM (Back scattering electron) images of $Mg_{0.95}In_{0.05}$-5 wt% CeF_3 nanocomposite. (a) and (b) ball milled powders, (c) hydrogenated $Mg_{0.95}In_{0.05}$-5 wt% CeF_3 nanocomposite.

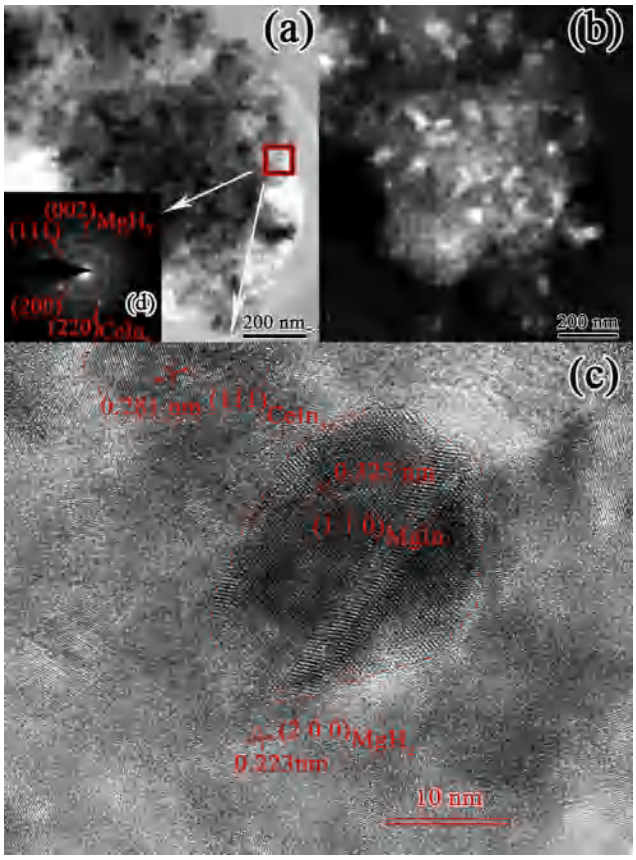

Fig. 3 – STEM images of the hydrogenated $Mg_{0.95}In_{0.05}$-5 wt % CeF_3 nanocomposite, (a) bright field (BF) image, (b) high-angle annular dark field (HAADF) image, (c) high resolution image, (d) selected area electron diffraction patterns.

milled to nano size. Fig. 2(b) is the enlarged one particle. It shows that the CeF_3 nanoparticles are homogeneously dispersed in the Matrix of Mg(In) solid solution. Fig. 2(c) shows the morphology of the hydrogenated $Mg_{0.95}In_{0.05}$-5 wt% CeF_3 nanocomposite. The bright nanoparticles are the intermetallic compounds of MgIn and $CeIn_3$ precipitated by hydrogenation. From Fig. 2(c) it is obviously observed that MgIn and $CeIn_3$ are homogeneously dispersed in the matrix of MgH_2, and keeping high nanostructure stability during the hydrogen absorption and desorption process. Comparing with Mg(In) binary solid solutions, for the $Mg_{0.95}In_{0.05}$-5 wt% CeF_3 nanocomposite the precipitated MgIn is much smaller in particle size and disperses more homogeneously in the matrix of MgH_2, indicating that the agglomeration of MgIn is constrained by the symbiotic intermetallic compound of $CeIn_3$. Fig. 3(a) and (b) are the bright field (BF) and high-angle annular dark field (HAADF) images for the hydrogenated $Mg_{0.95}In_{0.05}$-5 wt% CeF_3 nanocomposite, which further confirm that the intermetallic compounds of MgIn and $CeIn_3$ are nanostructure and dispersively embed in the matrix of MgH_2. Fig. 3(c) and (d) are the high resolution transmission electron image and selected area electron diffraction patterns respectively, from which MgH_2, MgIn and $CeIn_3$ were all confirmed in the hydrogenated $Mg_{0.95}In_{0.05}$-5 wt% CeF_3 nanocomposite. The results are consistent with the XRD analysis as shown in Fig. 1 (b).

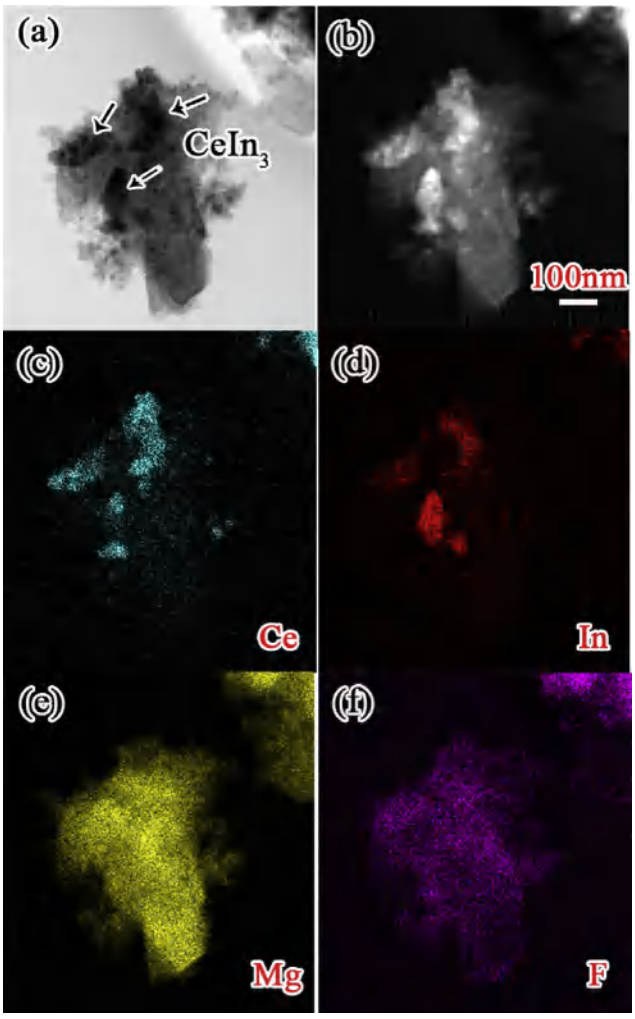

Fig. 4 – STEM images together with the corresponding element mapping for hydrogenated $Mg_{0.95}In_{0.05}$-5 wt% CeF_3 nanocomposite. (a) BF image, (b) HAADF image.

Additionally the amorphous/nanocrystalline MgH_2 is found around the hydrogenation precipitates (MgIn or $CeIn_3$). Fig. 4 illustrates the BF and HAADF images together with the corresponding element mapping for the hydrogenated $Mg_{0.95}In_{0.05}$-5 wt% CeF_3 nanocomposite. Fig. 4(a) is the BF image, and Fig. 4(b) is the corresponding HAADF image. Fig. 4(c) is the mapping of element Ce, which is highly overlapped with the mapping of element In (Fig. 4(d)), indicating that the dark particles in Fig. 4(a) (corresponding to the bright particles in Fig. 4(b)) are the intermetallic compound of $CeIn_3$. The mapping of Mg (Fig. 4(e)) and F (Fig. 4(f)) confirms the existence of MgF_2 which covers on the surface of the particles with nanostructure. The SEM and STEM analysis reveal that the intermetallic compound of $CeIn_3$ is nanostructure, which benefits to inhibit the growth of MgIn and MgH_2.

Based on the above phase analysis, it is considered that the ball milled $Mg_{0.95}In_{0.05}$-5 wt% CeF_3 nanocomposite firstly absorbs hydrogen to transform to MgH_2, MgF_2 and intermetallic compounds of MgIn and $CeIn_3$; conversely the decomposition of MgH_2 involves the intermetallic compounds of MgIn and $CeIn_3$ to form a pseudo-ternary Mg(In, Ce) solid solution, which is a reversible de/hydriding reaction. The de/hydriding reaction of $Mg_{0.95}In_{0.05}$-5 wt% CeF_3 nanocomposite can be described as:

$$\text{firt:} Mg(In) + CeF_3 + H_2 \rightarrow MgH_2 + MgIn + CeIn_3 + MgF_2 \quad (1)$$

$$\text{then:} Mg(In, Ce) + H_2 + MgF_2 \leftrightarrow MgH_2 + MgIn + CeIn_3 + MgF_2 \quad (2)$$

Kinetics of hydrogen absorption and desorption

Fig. 5 shows the isothermal hydriding and dehydriding curves of $Mg_{0.95}In_{0.05}$-5 wt% CeF_3 nanocomposite at different temperatures. The nanocomposite shows much faster hydrogen absorption rate than hydrogen desorption rate. But both the hydriding and dehydriding rates of $Mg_{0.95}In_{0.05}$-5 wt% CeF_3 nanocomposite are faster than those for the corresponding $Mg_{0.95}In_{0.05}$ solid solution alloy without doped with CeF_3. The hydrogen uptake content reached the maximum of 3.5 wt% in 20 min at 230 °C, but it only needed about 10 min to absorb 3.5 wt% H_2 when the hydriding temperature was elevated to 260 °C. However, it needed more than 30 min to release hydrogen at 260 °C. On the other hand, from Fig. 5(a) it can be

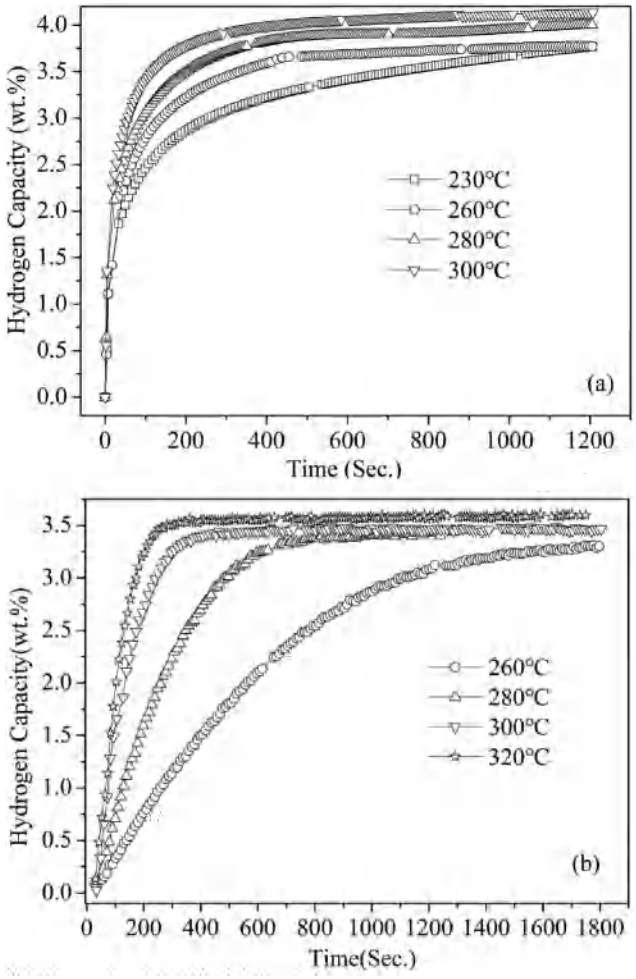

Fig. 5 – Isothermal hydrogen absorption and desorption of $Mg_{0.95}In_{0.05}$-5 wt% CeF_3 nanocomposite. (a) hydrogen absorption, (b) hydrogen desorption.

observed that the hydrogen uptake content has an obvious increase (increasing to about 4.0 wt%) with the improvement of hydriding kinetics when the temperature increased to 280 °C, indicating a progress of the hydrogenation degree. It is well known that the diffusion rate of H atoms is far lower in MgH_2 than in Mg [24]. So the hydrogen absorption will be impeded and result in incomplete hydrogenation when the surface of powders is covered by a continuous layer of impermeable MgH_2. However the diffusion rate can be accelerated by the elevation of reaction temperature. And it could be also related to the formation of $Mg(H_xF_{1-x})_2$ as reported by Pighin [54]. As a result, the hydrogen uptake content increased with the elevated hydriding temperature in the experiment. For dehydrogenation, the reaction had a significant speeded-up by elevating the dehydriding temperature, as shown in Fig. 5(b). The hydrogen release time was reduced from 30 min to about 10 min by elevating the temperature from 260 °C to 280 °C.

The sorption datum shown in Fig. 5(a) were fitted using Johnson-Mehl-Avrami-Kolmogorov (JMAK) equation:

$$\alpha = 1 - \exp(1 - \kappa t)^{\eta} \quad (3)$$

where α is the reaction fraction, κ is the reaction rate, t is the reaction time, and η is the reaction exponent. JMAK equation is turned into the linear form as:

$$\ln[-\ln(1-\alpha)] = \eta \ln(\kappa) + \eta \ln(t) \quad (4)$$

the linear plots of α *and* t were gotten in Fig. 6(a), from which κ values of different temperature were achieved and used to calculate the apparent activation energy (E_a) by Arrhenius equation:

$$\kappa = K_0 e^{-\left(\frac{E_a}{RT}\right)} \quad (5)$$

It can be changed into the form as following:

$$\ln(\kappa) = -\frac{Ea}{RT} + \ln(K_0) \quad (6)$$

By this form the linear plots of $\ln(\kappa)$ and T^{-1} were achieved and illustrated in Fig. 6(b). The apparent activation energy of hydrogen absorption was calculated to be 34.1 ± 1.9 kJ·mol^{-1} H_2 for $Mg_{0.95}In_{0.05}$-5 wt% CeF_3 nanocomposite, a notable decrease in comparing with the value of 48.1 kJ·mol^{-1} H_2 for $Mg_{0.95}In_{0.05}$ solid solution [51]. Through the same method the apparent activation energy of hydrogen desorption was determined to be 71.9 ± 10.0 kJ·mol^{-1} H_2 (as shown in Fig. 7), lowered about 73 kJ·mol^{-1} H_2 than 145 kJ·mol^{-1} H_2 for $Mg_{0.95}In_{0.05}$ solid solution un-doped with CeF_3 [51].

The dehydriding mechanism of $Mg_{0.95}In_{0.05}$-5 wt% CeF_3 nanocomposite is similar with that of $Mg_{0.95}In_{0.05}$ solid solution, the decomposition of MgH_2 involves the intermetallic compounds of MgIn and $CeIn_3$ to form pseudo-ternary Mg(In, Ce) solid solution and lease H_2. This means that the de/hydrogenation involves the diffusion of H atoms as well as In and Ce atoms in the Mg/MgH_2 lattice, which can be influenced by the microstructure characteristics, such as the grain/particle size, phase distribution and the interfaces. Previously it had been noticed that multi-phase microstructures with fine grain/particle size is beneficial to the diffusion of H and In atoms, and thus achieving kinetic improvement in the Mg–In–Al ternary system [51]. In the present work, the precipitated intermetallic compounds of MgIn and $CeIn_3$ were all nanostructure, and there were also some amorphous/nanocrystalline MgH_2, e.g. around the intermetallic compounds of MgIn and $CeIn_3$, as observed by STEM. Certainly these nanostructures are favorable for atom diffusing, thus accelerating the dehydriding reaction. On one hand, these nano grains also provide abundant boundaries/interfaces and defect sites which have been cited as important components for improving the kinetics of Mg-based materials [17,49]. On the other hand, the nanosized MgIn and $CeIn_3$ readily trigger the decomposition of MgH_2, once MgH_2 decomposes to elemental Mg and H_2, MgIn and $CeIn_3$ will incorporate the elemental Mg to form Mg(In, Ce) solid solution, which in turn further accelerates the decomposition of MgH_2 [6,51]. Therefore, the intermetallic compounds of MgIn and $CeIn_3$

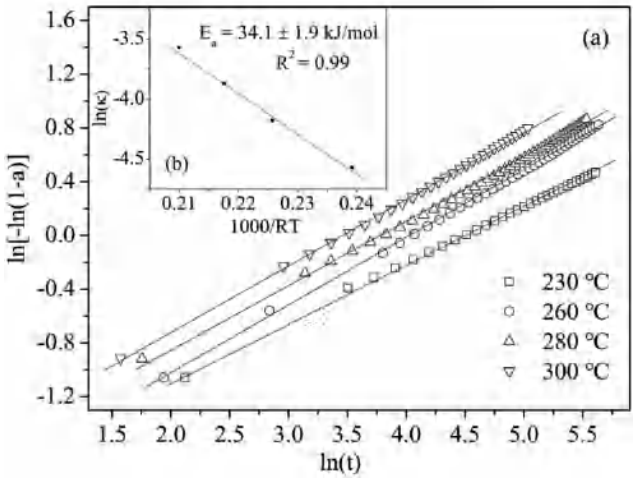

Fig. 6 – (a) the linear plots of $\ln[-\ln(1-\alpha)]$ vs $\ln(t)$ and (b) the Arrhenius plot for hydrogen absorption of $Mg_{0.95}In_{0.05}$-5 wt% CeF_3 nanocomposite.

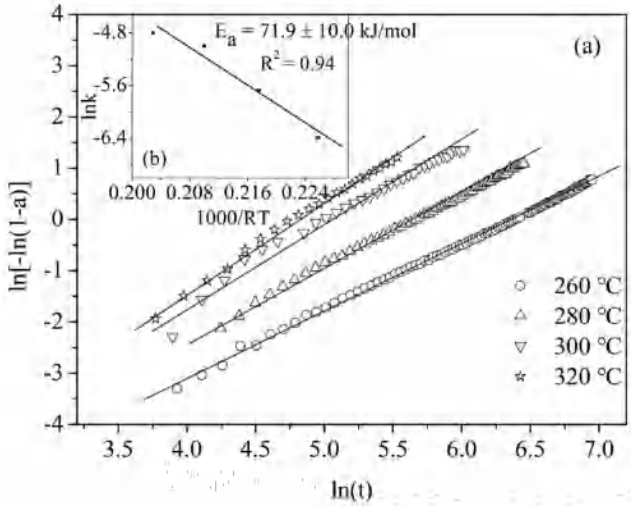

Fig. 7 – (a) the linear plots of $\ln[-\ln(1-\alpha)]$ vs $\ln(t)$ and (b) the Arrhenius plot for hydrogen desorption of $Mg_{0.95}In_{0.05}$-5 wt% CeF_3 nanocomposite.

accelerate the decomposition of MgH_2. Additionally, the surface of powders covered by a layer of amorphous MgF_2, which could hinder the formation of continuous H-impermeable MgO, and help H atoms to penetrate to the internal of particles by forming $Mg(H_xF_{1-x})_2$. This amorphous MgF_2 possibly also has catalytic effects on hydrogen absorption and desorption of Mg as reported in Ref. [55]. At last but not the least, although cerium hydrides were not found in the hydrogenated $Mg_{0.95}In_{0.05}$-5 wt% CeF_3 nanocomposite, however the multivalent cerium could facilitate the diffusion and delivery of H atoms, thus accelerating the formation and decomposition of H_2 molecules [31,39]. That is to say the introduction of $CeIn_3$ plays an important role in improving the hydrogen absorption and desorption properties.

Thermodynamics of hydrogen absorption and desorption

It is expected that the reversible phase transition of Mg(In, Ce) solid solution benefits to destabilize MgH_2 as Mg(Al), Mg(In) and Mg(In, Al) solid solutions [6,13,51]. Generally the de/hydriding thermodynamics is evaluated through PCI measurements. Fig. 8 shows the PCI curves of $Mg_{0.95}In_{0.05}$-5 wt% CeF_3 nanocomposite, and the comparison of PCI for $Mg_{0.95}In_{0.05}$ solid solution doped and un-doped with CeF_3 at 280 °C. For $Mg_{0.95}In_{0.05}$-5 wt% CeF_3 nanocomposite, the lag of hydrogen absorption and desorption is reduced, and the plateau pressures are elevated, as illustrated in Fig. 8(b). And there was also another outstanding feature that about 0.5 wt% hydrogen released above the dehydriding plateau for $Mg_{0.95}In_{0.05}$-5 wt% CeF_3 nanocomposite, which could be corresponding to the decomposition of amorphous MgH_2 around the intermetallic compounds of MgIn and $CeIn_3$. The reduced lag is mainly attributed to the improved de/hydriding kinetics as discussed in above. However, the elevated plateau pressures definitely indicate a lowered thermodynamics of MgH_2.

The equilibrium plateau pressure of metal hydrides is dependent on the reaction enthalpy (ΔH) and entropy (ΔS), both of which can be calculated by van't Hoff equation:

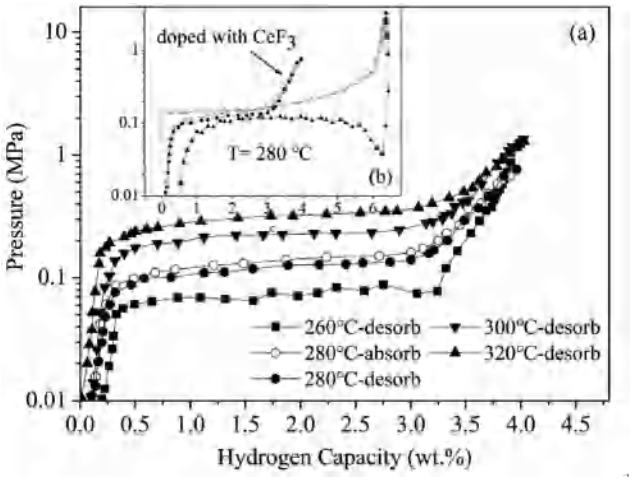

Fig. 8 – (a) the pressure-composition isotherm (PCI) curves of $Mg_{0.95}In_{0.05}$-5 wt% CeF_3 nanocomposite, (b) the comparison of PCI for $Mg_{0.95}In_{0.05}$ solid solution doped and un-doped with 5 wt% CeF_3.

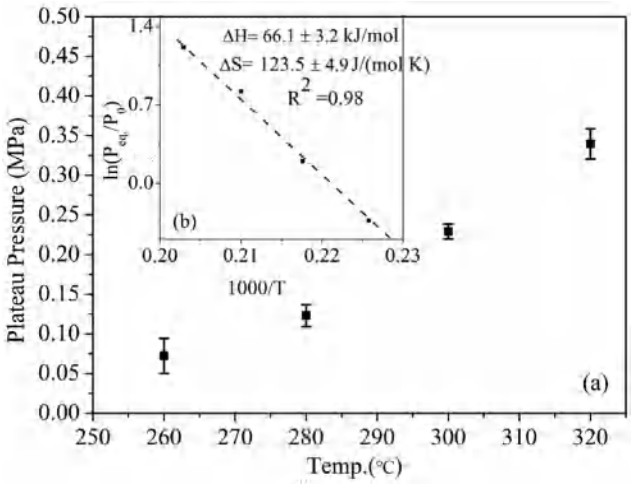

Fig. 9 – (a) the dehydriding plateau pressures and (b) van't Hoff plot for $Mg_{0.95}In_{0.05}$-5 wt% CeF_3 nanocomposite.

$$\ln\left(\frac{P_{eq.}}{p_0}\right) = \frac{\Delta H}{RT} - \frac{\Delta S}{R} \quad (7)$$

here, P_{eq} is the equilibrium plateau pressure, which was taken the average value of the dehydriding plateau pressures (corresponding to the pressure of midpoint at the plateau), the results are shown in Fig. 9(a), p_0 is the standard atmospheric pressure, R is the gas constant (8.31 J K^{-1} mol^{-1}), and T is the Kelvin temperature. The van't Hoff plot shows a linear relationship between the equilibrium pressures and the reaction temperatures as illustrated in Fig. 9(b). The calculated ΔH and ΔS for dehydriding reaction is 66.1 ± 3.2 kJ·$mol^{-1}H_2$ and 123.5 ± 4.9 J K^{-1} mol^{-1} H_2 respectively. The dehydriding enthalpy of $Mg_{0.95}In_{0.05}$-5 wt% CeF_3 nanocomposite is lower than 68.1 kJ·$mol^{-1}H_2$ for $Mg_{0.95}In_{0.05}$ solid solution un-doped with CeF_3 [51]. The lowered dehydriding enthalpy could be mainly attributed to the altered reaction pathways of MgH_2 due to the formations of Mg(In, Ce) solid solution and the intermetallic compounds of MgIn and $CeIn_3$, as Eq. (2). Recently, it was reported that the deformation of Magnesium lattice or plastic deformation could increase the hydrogen absorption and desorption plateau pressure and improve hydrogen absorption/desorption [56–58]. For $Mg_{0.95}In_{0.05}$-5 wt % CeF_3 nanocomposite, the dissolving of Ce and In (atomic radium larger than Mg) combining with the multiphase nanostructures generate severe lattice deformation, which helps to elevate the de/hydriding plateau pressures. And this deformation could also generate synergetic effects with the reversible phase transition on lowering the dehydriding enthalpy of MgH_2.

Conclusions

The de/hydriding mechanism of $Mg_{0.95}In_{0.05}$ solid solution is changed by the introduction of CeF_3 through mechanical ball milling to form nanocomposite. $Mg_{0.95}In_{0.05}$-5 wt% CeF_3 nanocomposite absorbs hydrogen transiting to MgH_2, MgF_2 and the intermetallic compounds of MgIn and $CeIn_3$. Upon

dehydrogenation, MgH_2 reacts with the intermetallic compounds of MgIn and $CeIn_3$ forming pseudo-ternary Mg(In, Ce) solid solution with reduced dehydriding enthalpy of 66.1 ± 3.2 kJ·mol$^{-1}H_2$ and significantly lowered dehydriding activation energy of 71.9 ± 10.0 kJ·mol^{-1} H_2. The symbiotic $CeIn_3$ benefits to impede the agglomeration of MgIn, which improves the reversibility of de/hydrogenation of Mg(In, Ce) solid solution, and enhances the hydrogen absorption and desorption. The lowered dehydriding enthalpy is mainly attributed to the reversible phase transition of Mg(In, Ce) solid solution and the multiphase nanostructures. In summary, the hydrogen storage properties of Mg(In) solid solution alloy could be significantly improved by doped with CeF_3. And the results could serve as a new approach to improve the hydrogen storage properties of Mg based hydrogen storage materials.

Acknowledgements

This work was supported by the National Natural Science Foundation of China (51601090), the Natural Science Foundation of Fujian Province (2016J01266, 2018J01429), the Science and Technology Project of Education Department of Fujian Province (JZ160474), and the open fund of Fujian Provincial Key Laboratory of Functional Materials and Applications (Xiamen University of Technology).

REFERENCES

[1] Salvi BL, Subramanian KA. Sustainable development of road transportation sector using hydrogen energy system. Renew Sustain Energy Rev 2015;51:1132–55.
[2] Schlapbach L, Züttel A. Hydrogen-storage materials for mobile applications. Mater Sust Energy 2010:265–70. https://doi.org/10.1142/7848.
[3] Lai QW, Paskevicius M, Sheppard DA, et al. Hydrogen storage materials for mobile and stationary applications: current state of the art. Chem Sus Chem 2015;8(17):2789–825.
[4] Chen P, Xiong ZT, Luo JZ, Lin JY, Tan KL. Interaction of hydrogen with metal nitrides and imides. Nature 2002;420:302–4.
[5] Vajo JJ, Skeith SL, Mertens F. Reversible storage of hydrogen in destabilized LiBH4. J Phys Chem B 2005;109(9):3719–22.
[6] Zhong HC, Wang H, Liu JW, Sun DL, Zhu M. Altered desorption enthalpy of MgH_2 by the reversible formation of Mg(In) solid solution. Scr Mater 2011;65:285–7.
[7] Qiu SJ, Ma XY, Wang ER, Chu HL, Huot J, et al. Enhanced hydrogen storage properties of $2LiNH_2/MgH_2$ through the addition of $Mg(BH_4)_2$. J Alloy Comp 2017;704:44–50.
[8] Li YT, Ding XL, Wu FL, Sun DL, Zhang QA, Fang F. Enhancement of hydrogen storage in destabilized $LiNH_2$ with $KMgH_3$ by quick conveyance of N-containing species. J Phys Chem C 2016;120(3):1415–20.
[9] Zhong HC, Xu JB. Tuning the de/hydriding thermodynamics and kinetics of Mg by mechanical alloying with Sn and Zn. Int J Hydrogen Energy 2019;44:2926–33.
[10] Qiu SJ, Chu HL, Zou YJ, Xiang CL, Xu F, Sun LX. Light metal borohydrides/amides combined hydrogen storage systems: composition, structure and properties. J Mater Chem A 2017;5:25112–30.
[11] Chen CG, Wang JL, Wang H, Liu T, Xu L, Li XG. Improved kinetics of nanoparticle-decorated Mg-Ti-Zr nanocomposite for hydrogen storage at moderate temperatures. Mater Chem Phys 2018;206:21–8.
[12] Paskevicius M, Tian HY, Sheppard DA, Webb CJ, et al. Magnesium hydride formation within carbon aerogel. J Phys Chem C 2011;115:1757–66.
[13] Zhong HC, Wang H, Ouyang LZ. Improving the hydrogen storage properties of MgH_2 by reversibly forming Mg-Al solid solution alloys. Int J Hydrogen Energy 2014;39:3320–6.
[14] Li JD, Li B, Yu XQ, Zhao HJ, Shao HY. Geometrical effect in Mg-based metastable nano alloys with BCC structure for hydrogen storage. Int J Hydrogen Energy 2019. https://doi.org/10.1016/j.ijhydene.2019.01.031.
[15] Lu YS, Wang H, Liu JW, Ouyang LZ, Zhu M. Destabilizing the dehydriding thermodynamics of MgH_2 by reversible intermetallics formation in Mg-Ag-Zn ternary alloys. J Power Sources 2018;396:796–802.
[16] Zhou C, Fang ZZ, Lu J, Zhang X. Thermodynamic and kinetic destabilization of magnesium hydride using Mg-in solid solution alloys. J Am Chem Soc 2013;135:10982–5.
[17] House SD, Vajo JJ, Ren C, Rockett AA, Robertson IM. Effect of ball-milling duration and dehydrogenation on the morphology, microstructure and catalyst dispersion in Ni-catalyzed MgH_2 hydrogen storage materials. Acta Mater 2015;86:55–68.
[18] Chen M, Xiao XZ, Zhang M, Liu MJ, et al. Excellent synergistic catalytic mechanism of in-situ formed nanosized Mg_2Ni and multiple valence titanium for improved hydrogen desorption properties of magnesium hydride. Int J Hydrogen Energy 2019;44:1750–9.
[19] Chen J, Xia GL, Guo ZP, Huang ZG, et al. Porous Ni nanofibers with enhanced catalytic effect on the hydrogen storage performance of MgH_2. J Mater Chem 2015;3:15843–8.
[20] Lan ZQ, Sun ZZ, Ding YC, et al. Catalytic action of Y_2O_3@graphene nanocomposites on the hydrogen storage properties of Mg-Al alloys. J Mater Chem 2017;5:15200–7.
[21] Lang CG, Ouyang LZ, Yang LL, Dai LY, Wu DF, Shao HY, Zhu M. Enhanced hydrogen storage kinetics in Mg@FLG composite synthesized by plasma assisted milling. Int J Hydrogen Energy 2018;43:17346–52.
[22] Zhong HC, Wang H, Ouyang LZ, Zhu M. Microstructure and hydrogen storage properties of Mg-Sn nanocomposite by mechanical milling. J Alloy Comp 2011;509:4268–72.
[23] Z Liu H, Wang XH, Liu YG, Dong ZH, et al. Hydrogen desorption properties of the MgH2–AlH3 composites. J Phys Chem C 2014;118(1):37–45.
[24] Xia GL, Tan YB, Chen XW, Sun DL, et al. Monodisperse magnesium hydride nanoparticles uniformly self-assembled on graphene. Adv Mater 2015;27(39):5981–8.
[25] Zhang JG, Zhu YF, Lin HJ, Liu YN, et al. Metal hydride nanoparticles with ultrahigh structural stability and hydrogen storage activity derived from microencapsulated nanoconfinement. Adv Mater 2017;29:1700760–5.
[26] Peng DD, Ding ZM, Zhang L, Fu YK, Wang JS, Li Y, Han SM. Remarkable hydrogen storage properties and mechanisms of the shell–core MgH_2@carbon aerogel microspheres. Int J Hydrogen Energy 2018;43:3731–40.
[27] Xie XB, Chen M, Liu P, Shang JX, Liu T. Synergistic catalytic effects of the Ni and V nanoparticles on the hydrogen storage properties of Mg-Ni-V nanocomposite. Chem Eng J 2018;347:145–55.
[28] Cui J, Liu J, Wang H, Ouyang LZ, Sun DL, Zhu M, et al. Mg-Tm (Tm: Ti, Nb, V, Co, Mo or Ni) core-shell like nanostructures: synthesis, hydrogen storage performance and catalytic mechanism. J Mater A 2014;2:9645–55.
[29] Polanski M, Bystrzycki J. Comparative studies of the influence of different nano-sized metal oxides on the hydrogen sorption properties of magnesium hydride. J Alloy Comp 2009;486:697–701.

[30] Lin HJ, Matsuda JK, Li HW, Zhu M, Akiba E. Enhanced hydrogen desorption property of MgH2 with the addition of cerium fluorides. J Alloy Comp 2015;645. S392-S39.
[31] Mao JF, Zou JX, Lu C, Zeng XQ, Ding WJ. Hydrogen storage and hydrolysis properties of core-shell structured Mg-MFx (M = V, Ni, La and Ce) nano-composites prepared by arc plasma method. J Power Sources 2017;366:131–42.
[32] Liang G, Huot J, Boily S, Neste AV, Schulz R. Catalytic effect of transition metals on hydrogen sorption in nanocrystalline ball milled MgH_2-Tm (Tm=Ti, V, Mn, Fe and Ni) systems. J Alloy Comp 1999;292:247–52.
[33] Korablov D, Besenbacher F, Jensen TR. Kinetics and thermodynamics of hydrogenation-dehydrogenation for Mg-25%TM(TM = Ti, Nb or V) composites synthesized by reactive ball milling in hydrogen. Int J Hydrogen Energy 2018;43:16804–14.
[34] Zhang X, Shen ZY, Pan HG, et al. A novel complex oxide $TiVO_{3.5}$ as a highly active catalytic precursor for improving the hydrogen storage properties of MgH_2. Int J Hydrogen Energy 2018;43:23327–35.
[35] Yahya MS, Ismail M. Synergistic catalytic effect of $SrTiO_3$ and Ni on the hydrogen storage properties of MgH_2. Int J Hydrogen Energy 2018;43:6244–55.
[36] Sazelee NA, Idris NH, Ismail M, et al. Synthesis of $BaFe_{12}O_{19}$ by solid state method and its effect on hydrogen storage properties of MgH_2. Int J Hydrogen Energy 2018;43:20853–60.
[37] Ali NA, Idris NH, Ismail M, et al. Nanoflakes $MgNiO_2$ synthesised via a simple hydrothermal method and its catalytic roles on the hydrogen sorption performance of MgH_2. J Alloy Comp 2019;796:279–86.
[38] Ali NA, Idris Nurul Hayati, Ismail M, et al. Nanolayer-like-shaped $MgFe_2O_4$ synthesised via a simple hydrothermal method and its catalytic effect on the hydrogen storage properties of MgH_2. RSC Adv 2018;8:15667–74.
[39] Lin HJ, Tang JJ, Yu Q, Wang H, Ouyang LZ, et al. Symbiotic $CeH_{2.73}/CeO_2$ catalyst: a novel hydrogen pump. Nano Energy 2014;9:80–7.
[40] Shahi RR, Bhatanagar A, Pandey SK, et al. MgH_2-$ZrFe_2H_x$ nanocomposites for improved hydrogen storage characteristics of MgH_2. Int J Hydrogen Energy 2015;40:11506–13.
[41] Zhang LT, Cai ZL, Yao ZD, Chen LX, et al. A striking catalytic effect of facile synthesized $ZrMn_2$ nanoparticles on the de/rehydrogenation properties of MgH_2. J Mater Chem A 2019;(7):5626–34.
[42] Vajo JJ, Mertens F, Ahn CC, et al. Altering hydrogen storage properties by hydride destabilization through alloy formation: LiH and MgH_2 destabilized with Si. J Phys Chem B 2004;108:13977–83.
[43] Yang T, Wang P, Xia CQ, Li Q, Liang CY, Zhang YH. Characterization of microstructure, hydrogen storage kinetics and thermodynamics of a melt-spun $Mg_{86}Y_{10}Ni_4$ alloy. Int J Hydrogen Energy 2019;44:6728–37.
[44] Wagemans RW, van Lenthe JH, de Jongh PE, et al. Hydrogen storage in magnesium clusters: quantum chemical study. J Am Chem Soc 2005;127:16675–80.
[45] Khan D, Zou JX, Zeng XQ, Ding WJ. Hydrogen storage properties of nanocrystalline Mg2Ni prepared from compressed $2MgH_2$-Ni powder. Int J Hydrogen Energy 2018;43:22391–400.
[46] Kim H, Nakamura J, Shao H, Nakamura Y, Akiba E, et al. Insight into the hydrogenation properties of mechanically alloyed $Mg_{50}Co_{50}$ from the local structure. J Phys Chem C 2011;115:20335–41.
[47] Shao H, Asano K, Enoki H, Akiba E. Preparation and hydrogen storage properties of nanostructured Mg–Ni bcc alloys. J Alloy Comp 2009;477:301–6.
[48] Zhang QA, Zhang LX, Wang QQ. Crystallization behavior and hydrogen storage kinetics of amorphous $Mg_{11}Y_2Ni_2$ alloy. J Alloy Comp 2013;551:376–81.
[49] Liu JW, Zou CC, Wang H, et al. Facilitating de/hydrogenation by long-period stacking ordered structure in Mg based alloys. Int J Hydrogen Energy 2013;38:10438–45.
[50] Liang G. Synthesis and hydrogen storage properties of Mg-based alloys. J Alloy Comp 2004;370:123–8.
[51] Wang H, Zhong HC, Ouyang LZ, Liu JW, Sun DL, Zhang QA, Zhu M. Fully reversible de/hydriding of Mg base solid solutions with reduced reaction enthalpy and enhanced kinetics. J Phys Chem C 2014;118(23):12087–96.
[52] Ismail M, Mustafa NS, Juahir N, Halim Yap FA. Catalytic effect of $CeCl_3$ on the hydrogen storage properties of MgH_2. Mater Chem Phys 2016;170:77–82.
[53] Ismai M. Effect of $LaCl_3$ addition on the hydrogen storage properties of MgH_2. Energy 2015;79:177–82.
[54] Pighin SA, Coco B, Troiani H, Castro FJ, Urretavizcaya G. Effect of additive distribution in H_2 absorption and desorption kinetics in MgH_2 milled with $NbH_{0.9}$ orNbF_5. Int J Hydrogen Energy 2018;43:7430–9.
[55] Youn JS, Phan DT, Park CM, Jeon KJ. Enhancement of hydrogen sorption properties of MgH_2 with a MgF_2 catalyst. Int J Hydrogen Energy 2017;42:20120–4.
[56] Skryabina N, Medvedeva N, Gabov A, et al. Impact of severe plastic deformation on the stability of MgH_2. J Alloy Comp 2015;645:S14–7.
[57] Baldi A, Krishnan G, Kooi BJ, Dam B, Griessen R. Elastic versus alloying effects in Mg-based hydride films. Phys Rev Lett 2018;121:255503–11. 7.
[58] Ngene P, Longo A, Mooij L, Bras W, Dam B. Metal-hydrogen systems with an exceptionally large and tunable thermodynamic destabilization. Nat Commun 2017;8:1846–51. 8.